IEEE Access
Multidisciplinary | Rapid Review | Open Access Journal

Received September 20, 2019, accepted September 25, 2019, date of publication September 30, 2019,
date of current version October 11, 2019.

Digital Object Identifier 10.1109/ACCESS.2019.2944436

An Efficient Cycle-Slip Repair Model With High Success Rate for BDS Triple-Frequency Observations

YIFEI YAO[1,2], XIN ZHANG[1], AND XINYUN CAO[3]
[1]College of Water Resources and Architectural Engineering, Northwest A&F University, Yangling 712100, China
[2]Institute of Water-Saving Agriculture in Arid Areas of China, Northwest A&F University, Yangling 712100, China
[3]Key Laboratory of Virtual Geographic Environment (Nanjing Normal University), Ministry of Education, Nanjing 210023, China

Corresponding author: Xin Zhang (zhxin68@hotmail.com)

This work was supported in part by the National Natural Science Foundation of China under Grant 41804029 and Grant 41674008, and in part by a project funded by the Northwest A&F University under Grant 2452017234.

ABSTRACT An improved cycle-slip repair model is proposed for BDS triple-frequency undifferenced observations. Two extra-wide-lane code-phase combinations and one additional geometry-free (GF) carrier-phase combination are employed. To ensure the GF phase combination follows a normal distribution, the residual ionospheric variation of the GF phase combination is corrected in real-time using the previous observation sequence without cycle slip. The integer least squares principle, based on the least-squares ambiguity decorrelation adjustment, is used to solve the fixed value of cycle slip. The corresponding covariance matrix of floating cycle-slip estimations used for construction is updated in real time to improve the fixed efficiency of cycle slip. Moreover, for reliable repair of cycle slip for triple-frequency observations, the critical ratio value between the second-best and best cycle-slip candidates for different residual ionosphere accuracies and different repair success rates are given based on large amounts of simulated data. Lastly, a set of active ionosphere and low-sampling-rate real data was used for evaluation and analysis of the algorithm. Results showed the success rate of cycle-slip repair is 99.997%, even under active ionosphere conditions, with low satellite elevation and low sampling rate. Unfortunately, one cycle-slip group (1, 1, 1) of the C14 satellite was not detected successfully and repaired correctly because of insensitivity to the GF phase combination under bad observation conditions.

INDEX TERMS Cycle slip, triple-frequency observations, BDS, integer least squares, ionospheric delay.

I. INTRODUCTION

Cycle-slip detection and repair is an area of active research in precise positioning of global navigation satellite systems (GNSS). The triple-frequency signals in theory can improve the performance of cycle-slip detection and precise positioning compared with the traditional dual-frequency [1], [2]. In general, the linear combinations used for undifferenced cycle-slip detection and repair can be divided into two categories. The first category comprises the extra-wide-lane (EWL) code-phase combinations [2]–[4]. The marked advantage of these combinations is to guarantee the integer nature of the final combined cycle slips but with small errors benefit from their long wavelength. However, EWL combinations cannot determine the original cycle-slip independently because of the linear correlation of the excellent EWL combinations [4]–[7]. The second category includes the widely used geometry-free (GF) carrier-phase combinations [8]–[12]. Although the advantage of these combinations is their high accuracy due to the low carrier observation noise, the integer nature of the combined cycle slips is lacking. Each of these two types of combination can overcome the shortcomings of the other and therefore they are generally employed together [9], [12]–[21].

The efficiency of cycle-slip repair for both types of combination is evidently affected by ionospheric variation. For EWL code-phase combinations, the effect of residual ionospheric delays on cycle-slip repair can be diminished greatly by selecting a larger combined wavelength. However, the residual ionospheric variations have considerable

The associate editor coordinating the review of this manuscript and approving it for publication was Venkata Ratnam Devanaboyina.

influence on the accuracy of GF phase combinations, which might result in an incorrect cycle-slip value, especially under the active ionospheric conditions or the low satellite elevation [17], [18], [22], [23]. To compensate the increased between-epoch ionospheric variations, Li *et al.* [23], [24] predict the single-differenced ionospheric delays by using consecutive historical data of a sliding window with an adaptive polynomial order and window length. Similarly, Chang *et al.* [14] proposed a Kalman filtering model with consideration of the variance component to estimate the ionospheric variation and used it for cycle-slip repair. In addition, four types of improved ionospheric prediction model were evaluated [16] and a high success rate in cycle-slip repair was reported under both stable and active ionospheric conditions.

The following two strategies are usually used to fix cycle slip: direct rounding and the minimum norm criterion (including minimum one-norm and two-norm criteria). The first strategy performs simple rounding for the floating cycle-slip estimations to obtain a nearest integer. However, this method cannot achieve high performance because the rounding success rate is affected seriously by the deviation from the integer of the floating solution. When the deviation reaches approximately 0.5 cycles, the reliability of this method is expected to be very poor. Therefore, it is generally considered more reliable when the deviation is less than 0.3 cycles [25]–[28]. Another strategy is the classic least-squares ambiguity decorrelation adjustment (LAMBDA), which determines the optimal cycle-slip candidates using the floating solutions and a constrained search space [2], [12], [24], [29]–[31]. However, few studies using such an approach have discussed and analyzed whether the optimal solution is actually suitable, how large the threshold is. In addition, the constructed covariance matrix of the floating cycle-slip estimations does not consider the influence of the residual ionosphere on the optimal cycle-slip candidates.

The remainder of this paper is organized as follows. First, Section II.A describes the proposed model for triple-frequency cycle-slip detection and repair, which includes two EWL code-phase and one additional GF carrier-phase combination. Then, Section II.B provides a more reasonable decision condition to detect whether cycle slip occurs. In Section III, a cycle-slip repair evaluation model based on the integer least squares (ILS) theory, is presented and the selection of the critical threshold for reliable cycle-slip repair is discussed. In Section IV, real BDS-2 data are used to evaluate the efficiency of the improved cycle-slip repair model. Section V summarizes the derived research conclusions and it outlines future prospects.

II. CYCLE-SLIP DETECTION

A. CYCLE-SLIP DETECTION MODEL

The combinational observations of triple-frequency carrier-phase and code can be expressed as follows [4]–[7]:

$$\begin{aligned} L_{ijk} &= \lambda_{ijk}\varphi_{ijk} = \rho - \lambda_{ijk}N_{ijk} - \eta_{ijk}I_1 \\ &\quad +\delta_{orb} + c_r^s + B_{ijk} + \lambda_{ijk}\varepsilon_{ijk} \qquad (1) \\ R_{abc} &= \rho + \eta_{abc}I_1 + \delta_{orb} + c_r^s + b_{abc} + \varepsilon_{abc} \qquad (2) \end{aligned}$$

with

$$\begin{aligned} \lambda_{ijk} &= \lambda_1\lambda_2\lambda_3/\left(i\lambda_2\lambda_3 + j\lambda_1\lambda_3 + k\lambda_1\lambda_2\right) \\ N_{ijk} &= iN_1 + jN_2 + kN_3 \\ \eta_{ijk} &= \lambda_{ijk}/\lambda_1\left(i + j\lambda_2/\lambda_1 + k\lambda_3/\lambda_1\right) \\ \eta_{abc} &= a + b\left(\lambda_2/\lambda_1\right)^2 + c\left(\lambda_3/\lambda_1\right)^2 \\ \varepsilon_{ijk} &= i\varepsilon_1 + j\varepsilon_2 + k\varepsilon_3, \\ \varepsilon_{abc} &= ae_1 + be_2 + ce_3 \end{aligned}$$

where ρ is the frequency-independent term representing the geometrical distance between the receiver and satellite antenna phase center and the tropospheric delay; subscripts i, j, and k are the phase combinational scalars, which are integers that are not all zero; subscripts a, b, and c are the code combinational scalars, and $a+b+c=1$, which ensures the geometrical distance is invariant. To minimize the combined code noise, let $a = b = c = 1/3$. Here, λ_1, λ_2, and λ_3 are the wavelengths of each frequency and λ_{ijk} is the combined wavelength. The three frequencies of the BDS signal are B1 (1561.098 MHz), B2 (1207.14 MHz), and B3 (1268.52 MHz). Here, N_1, N_2, and N_3 are the ambiguities of each frequency and N_{ijk} represents the combined ambiguity. Parameter I_1 is the ionospheric delay of the B1 frequency; η_{ijk} and η_{abc} are ionospheric influence coefficients of the combinational phase and code, respectively; δ_{orb} and c_r^s represent orbit errors and clock error, respectively; B_{ijk} and b_{abc} are hardware delays of the phase and code combinations, respectively; ε_{ijk} and ε_{abc} represent the noise of the combinational phase and code, respectively.

In adjacent epochs, the epoch-differenced code-phase combination observations (also called the pseudorange minus phase linear combination in some studies) can be described:

$$\begin{aligned} \Delta N_{ijk,abc} = \left(\Delta R_{abc}/\lambda_{ijk} - \Delta\varphi_{ijk}\right) - \eta_{ijk,abc}\Delta I_1 \\ -\left(\Delta\varepsilon_{abc}/\lambda_{ijk} - \Delta\varepsilon_{ijk}\right) \qquad (3) \end{aligned}$$

with

$$\eta_{ijk,abc} = \left(\eta_{abc} + \eta_{ijk}\right)/\lambda_{ijk}$$

where Δ denotes the time difference between adjacent epochs, and $\Delta N_{ijk,abc}$ is the variation of the combinational ambiguity in adjacent epoch (called the combinational cycle-slip value). The code-phase combination can be obtained by the difference between Equations (2) and (1), eliminating the geometric distance, tropospheric delay, orbit error, and clock error. Furthermore, the influence of other errors such as hardware delay, code bias, and multipath error can be reduced greatly by the difference between adjacent epochs. Therefore, the combinational cycle slip of the code-phase combination is affected by both the residual ionospheric variation and the combined noise. If a larger combined wavelength is adopted, the influence of ionospheric variation on the rounding deviation of the combinational cycle slip is negligible and it can be ignored [18]. Here, the optimal code-phase combinations of (0, −1, 1) and (1, 4, −5) with smaller ionospheric coefficients, larger combined wavelength, and lower combined

noise are employed as the first and second detectable amounts of cycle slip [3]–[6], [32]. Ignoring the influence of ionosphere, the combined noise of the two EWL combinations are 0.09 and 0.11 cycles, respectively, and the rounding success rate is greater than 99.999% [16]. The combined wavelengths are 4.884 and 6.371 m, respectively. It means that the influence residual ionospheric variation of 0.1 m of the GF phase combination on the rounding deviation of the combinational cycle slip is less than 0.02 cycles.

As the sum of the integer coefficients of EWL combinations with small ionospheric coefficient is zero, any three EWL combinations are linearly dependent [4]. To solve this problem, a GF phase combination or narrow lane combination that is linearly independent of the EWL code-phase combinations must be introduced [17], [18]. The purpose of introducing such additional combination is the same and the GF phase combination is employed here. The corresponding observations can be expressed as [4]–[7]:

$$L_{\alpha\beta\gamma} = \alpha\lambda_1\varphi_1 + \beta\lambda_2\varphi_2 + \gamma\lambda_3\varphi_3 = -N_{\alpha\beta\gamma} - \eta_{\alpha\beta\gamma} I_1 + \varepsilon_{\alpha\beta\gamma} \tag{4}$$

with

$$\begin{aligned} N_{\alpha\beta\gamma} &= \alpha\lambda_1 N_1 + \beta\lambda_2 N_2 + \gamma\lambda_3 N_3 \\ \eta_{\alpha\beta\gamma} &= \alpha\lambda_1 + \beta\lambda_2^2/\lambda_1 + \gamma\lambda_3^2/\lambda_1 \\ \varepsilon_{\alpha\beta\gamma} &= \alpha\lambda_1\varepsilon_1 + \beta\lambda_2\varepsilon_2 + \gamma\lambda_3\varepsilon_3 \end{aligned}$$

where subscripts α, β, and γ are the combinational scalars. To eliminate the impact of geometrical distance and tropospheric delay, let $\alpha + \beta + \gamma = 0$. Parameters $N_{\alpha\beta\gamma}$, $\eta_{\alpha\beta\gamma}$, and $\varepsilon_{\alpha\beta\gamma}$ are the combinational ambiguity, ionospheric amplification factor, and combinational noise, respectively. In adjacent epochs, the detectable cycle-slip value $\Delta N_{\alpha\beta\gamma}$ based on epoch difference can be expressed as follows:

$$\Delta N_{\alpha\beta\gamma} = -\Delta L_{\alpha\beta\gamma} - \eta_{\alpha\beta\gamma}\Delta I_1 + \Delta\varepsilon_{\alpha\beta\gamma} \tag{5}$$

It can be seen from Equation (5) that the cycle-slip value of the GF phase combination is affected mainly by the residual ionospheric variation. Therefore, the employed GF phase combination coefficients should satisfy small values of $\eta_{\alpha\beta\gamma}$ and combined noise. In this paper, the more optimal GF phase combination (1, −1, 0) with small values of $\eta_{\alpha\beta\gamma}$ and combined noise is employed as the third cycle-slip detection amount. The ionospheric amplification factor and combined noise are −0.129 and 0.0044 m, respectively. In addition, it is helpful to improve the accuracy of the GF combination using the ionospheric prediction with high accuracy, which can further improve the efficiency of cycle-slip detection and repair. Yao *et al.* [16] proposed four types of algorithm for improving the prediction model. In this paper, a simple sliding window mean (SWM) algorithm is adopted because the method is easy to operate and it can achieve better results. The ionosphere prediction model can be expressed as follows:

$$\eta_{\alpha\beta\gamma}\Delta I_1^k = \frac{1}{m}\sum_{i=1}^{m}\eta_{\alpha\beta\gamma}\Delta I_1^{k-i} \tag{6}$$

where superscript k denotes the current epoch location and m denotes the number of smoothed epochs (a small value is appropriate when the ionosphere is active, and vice versa). As previous observations have no cycle slip, we can obtain the preceding ionospheric variation sequence for prediction of subsequent ionospheric variation. To eliminate or greatly reduce the influence of other errors, and to improve the accuracy of the estimated ionospheric variation, the following equation is constructed to solve the preceding ionospheric variation sequence:

$$\begin{bmatrix} \lambda_1\Delta\varphi_1 - \lambda_2\Delta\varphi_2 \\ \lambda_1\Delta\varphi_1 - \lambda_3\Delta\varphi_3 \end{bmatrix} = \begin{bmatrix} -1+\lambda_2^2/\lambda_1^2 \\ -1+\lambda_3^2/\lambda_1^2 \end{bmatrix}\Delta I_1 + \begin{bmatrix} \Delta\varepsilon_1+\Delta\varepsilon_2 \\ \Delta\varepsilon_1+\Delta\varepsilon_3 \end{bmatrix} = \mathbf{C}\cdot\Delta I_1 + \Delta\varepsilon \tag{7}$$

where ΔI_1 is the ionospheric variation of the B1 frequency. If there is an unreliable cycle-slip repair value in the current epoch, we can only mark the epoch and skip the ionospheric estimation of this epoch; otherwise, it would reduce the accuracy of the ionospheric correction.

In summary, two code-phase combinations and one additional GF phase combination are employed to solve the original cycle-slip value, and the resolving equation is constructed as follows:

$$\boldsymbol{A}\cdot\Delta\boldsymbol{N} = \Delta\boldsymbol{L} \tag{8}$$

where $\boldsymbol{A} = \begin{bmatrix} i_1 & j_1 & k_1 \\ i_2 & j_2 & k_2 \\ \alpha\lambda_1 & \beta\lambda_2 & \gamma\lambda_3 \end{bmatrix}$, $\Delta\boldsymbol{N} = \begin{bmatrix} \Delta N_1 \\ \Delta N_2 \\ \Delta N_3 \end{bmatrix}$ and $\Delta\boldsymbol{L} = \begin{bmatrix} \Delta L_{i_1j_1k_1} \\ \Delta L_{i_2j_2k_2} \\ \Delta L_{\alpha\beta\gamma} \end{bmatrix}$.

Then, the floating solution of the original cycle slip can be solved as:

$$\Delta\boldsymbol{N} = \boldsymbol{A}^{-1}\cdot\Delta\boldsymbol{L} \tag{9}$$

The corresponding covariance matrix of the cycle-slip solutions can be expressed as:

$$\boldsymbol{Q}_{\Delta N} = \left(\boldsymbol{A}^T\cdot\boldsymbol{Q}_{\Delta L}^{-1}\cdot\boldsymbol{A}\right)^{-1} \tag{10}$$

In Equation (8), three detectable cycle-slip amounts can be expressed as:

$$\Delta\boldsymbol{L} = \boldsymbol{B}\cdot\Delta\boldsymbol{L}' \tag{11}$$

where $\boldsymbol{B} = \begin{bmatrix} i_1 & j_1 & k_1 & -\frac{1}{3\lambda_{i_1j_1k_1}} & -\frac{1}{3\lambda_{i_1j_1k_1}} & -\frac{1}{3\lambda_{i_1j_1k_1}} \\ i_2 & j_2 & k_2 & -\frac{1}{3\lambda_{i_2j_2k_2}} & -\frac{1}{3\lambda_{i_2j_2k_2}} & -\frac{1}{3\lambda_{i_2j_2k_2}} \\ \alpha\lambda_1 & \beta\lambda_2 & \gamma\lambda_3 & 0 & 0 & 0 \end{bmatrix}$ and $\Delta\boldsymbol{L}' = \begin{bmatrix} \Delta\varphi_1 & \Delta\varphi_2 & \Delta\varphi_3 & \Delta p_1 & \Delta p_2 & \Delta p_3 \end{bmatrix}^T$.

The corresponding covariance matrix of the three combinational observations can be expressed as:

$$\boldsymbol{Q}_{\Delta L} = \boldsymbol{B}\cdot\boldsymbol{Q}_{\Delta L'}\cdot\boldsymbol{B}^T \tag{12}$$

with

$$\boldsymbol{Q}_{\Delta L'} = 2\cdot\mathrm{diag}\left(\sigma_\varphi^2\ \sigma_\varphi^2\ \sigma_\varphi^2\ \sigma_p^2\ \sigma_p^2\ \sigma_p^2\right)$$

where, parameters σ_φ and σ_p are the mean square error of the phase and code observations, respectively. In the above equation, it is assumed that the carrier-phase and code of the three frequencies have the same observation noise.

B. CRITERION OF CYCLE-SLIP OCCURRENCE

Given the large rounding success rate of the EWL combination, a non-zero value is generally adopted as the critical condition for whether cycle slip occurs. However, this strategy has one insensitive cycle-slip group, i.e., $\Delta N_1 = \Delta N_2 = \Delta N_3$. Therefore, an additional constraint is usually added to detect residual insensitive cycle-slip groups, which is several times larger than the standard deviation (STD) error of the residual GF phase combination value. The magnitude of this multiple, which directly affects the number of missed detections and false detections, is generally greater than or equal to 3 [12], [26]–[28]. Therefore, the conditions for the occurrence of cycle slip are as follows:

$$\begin{cases} \text{round}(\Delta \boldsymbol{L}_{ijk}) \neq 0, & \text{the first five epochs} \\ \text{round}(\Delta \boldsymbol{L}_{ijk}) \neq 0, & \text{or } \left|\Delta \boldsymbol{L}_{\alpha\beta\gamma}\right| \geq \kappa \cdot \sigma_{GF}, \text{ other epochs} \end{cases} \tag{13}$$

where round( ) denotes the direct rounding for the floating value, and $\Delta \boldsymbol{L}_{ijk}$ denotes the EWL_1 and EWL_2 code-phase combinations. Parameter σ_{GF} is the STD of the GF phase combination observations after correcting the residual ionosphere. In Equation (13), a large criticality threshold (here, $\kappa = 4$ [11]) is adopted. Only EWL combinations are employed in detection if cycle slip occurs in the first five epochs. The first reason is the corresponding residual ionosphere might be so large that the estimated cycle-slip value is incorrect at the beginning of the epochs. Moreover, the predicted ionosphere cannot be obtained to correct the GF phase combination observations at the beginning of the epochs. Finally, additional epoch data are necessary to update a more stable and reliable σ_{GF} of the GF phase combination observations.

III. CYCLE-SLIP REPAIR BASED ON ILS

A. CRITERION FOR CORRECT CYCLE-SLIP REPAIR

The goal common to cycle-slip repair and ambiguity resolution is the determination of integer parameters. For ambiguity resolution, the ambiguity parameters are strongly correlated with other unknown parameters, e.g., position parameters. However, because of the adopted different combination of observation values, the estimated parameters are usually only cycle-slip values of three frequencies, and the correlation of the estimated parameters is weaker than that of the ambiguity resolution. To solve this problem, integer bootstrapping and ILS are usually employed to obtain the optimal parameter estimation. To reduce the correlation of parameters and to obtain a better search space, the LAMBDA method [24], [31], [33], [34] is used to estimate the integer fixed solution of cycle slip.

Before adopting the LAMBDA model, the residual ionospheric variation, which is a systematic error, must be corrected using Equation (6); otherwise, the precondition of the LAMBDA model is not established, greatly reducing its efficiency. In addition, the structure of the covariance matrix of the three combinational observations in Equation (12) has to consider the influence of stochastic noise after correcting the ionospheric variation as follows:

$$\boldsymbol{Q}_{\Delta L} = \boldsymbol{B} \cdot \boldsymbol{Q}_{\Delta L'} \cdot \boldsymbol{B}^T + \boldsymbol{Q}_{\Delta I} \tag{14}$$

where $\boldsymbol{Q}_{\Delta I}$ is the covariance matrix of the corrected ionosphere of the three combination observations. It should be noted that the influence of the corrected ionosphere of EWL combination observations is negligible and can be discounted. Thus, the matrix can be constructed as:

$$\boldsymbol{Q}_{\Delta I} = \begin{bmatrix} 0 & 0 & 0 \\ 0 & 0 & 0 \\ 0 & 0 & \sigma_{\Delta I}^2 \end{bmatrix} \tag{15}$$

where $\sigma_{\Delta I}$ is the STD of the corrected ionosphere $\eta_{\alpha\beta\gamma}\Delta I_1$ of GF phase combination observations, which is generally in the range 0.003–0.007 m under different ionospheric conditions (i.e., stable or active) and different satellite elevation (i.e., $>30°$ or $<30°$) [16]. In addition, it should be emphasized that the ionospheric correction is irrelevant to the EWL and GF combination observations in the current epoch because it is solved by the previous observations sequence.

The LAMBDA method is employed to perform decorrelation between the floating cycle slips $\Delta \boldsymbol{N}_{\text{flo}}$, to determine the best and second-best integer candidates ($\Delta \boldsymbol{N}_{\text{bes}}$ and $\Delta \boldsymbol{N}_{\text{sec}}$) of the fixed cycle-slips $\Delta \boldsymbol{N}_{\text{fix}}$. The LAMBDA model introduces a transformation matrix as follows:

$$\Delta \boldsymbol{N}^{'} = \boldsymbol{Z} \cdot \Delta \boldsymbol{N}_{flo}, \quad \boldsymbol{Q}_{\Delta N'} = \boldsymbol{Z} \cdot \boldsymbol{Q}_{\Delta N_{flo}} \cdot \boldsymbol{Z}^T \tag{16}$$

where $\boldsymbol{Z}$ is the transformation matrix with $\det(Z) = 1$. Here, $\Delta \boldsymbol{N}^{'}$ and $\boldsymbol{Q}_{\Delta N'}$ are the floating solution and the corresponding covariance matrix after transformation, respectively. The best integer candidates of the fixed cycle slips as the repaired value of the original carrier-phase observations should conform to the following equation:

$$\left(\Delta \boldsymbol{N}_{\text{bes}} - \Delta \boldsymbol{N}^{'}\right)^{\boldsymbol{T}} \boldsymbol{Q}_{\Delta \boldsymbol{N}'}^{-1} \left(\Delta \boldsymbol{N}_{\text{bes}} - \Delta \boldsymbol{N}^{'}\right) = \min \tag{17}$$

However, the best integer candidates are simply optimal estimation solutions that might not be correct solutions. Therefore, the principle of correctly repairing cycle slip is critical; otherwise, an incorrect cycle-slip repair value will aggravate the original carrier-phase observations.

Verhagen [35] compared and analyzed several classic test statistics, including the most widely used ratio test. If the equation below is satisfied, then the best estimation solution is acceptable:

$$\frac{\left(\Delta \boldsymbol{N}_{\text{sec}} - \Delta \boldsymbol{N}^{'}\right)^{\boldsymbol{T}} \boldsymbol{Q}_{\Delta \boldsymbol{N}'}^{-1} \left(\Delta \boldsymbol{N}_{\text{sec}} - \Delta \boldsymbol{N}^{'}\right)}{\left(\Delta \boldsymbol{N}_{\text{bes}} - \Delta \boldsymbol{N}^{'}\right)^{\boldsymbol{T}} \boldsymbol{Q}_{\Delta \boldsymbol{N}'}^{-1} \left(\Delta \boldsymbol{N}_{\text{bes}} - \Delta \boldsymbol{N}^{'}\right)} \geq c \tag{18}$$

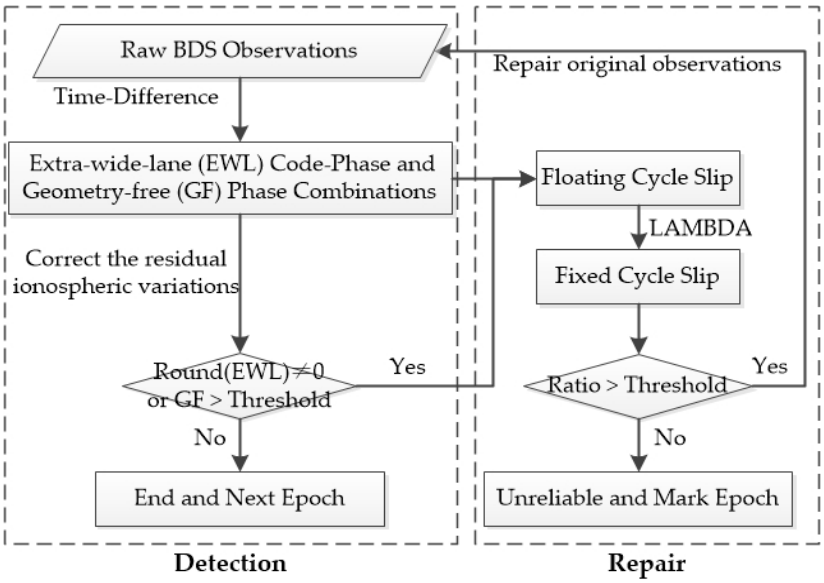

FIGURE 1. Process of cycle-slip detection and repair for triple-frequency observations.

where c is the critical value (called the threshold value in this study), reported in the range 1.5–3.0 in different studies [36]–[39], which is affected by factors such as the baseline length, number of visible satellites and frequencies, and atmospheric delay in terms of ambiguity fixed theory. In addition, compared with other test statistics, this ratio test obtains better results in practical experiments for fixed ambiguities [35]. Therefore, Equation (18) is employed to evaluate whether the best integer candidates of cycle slip are reliable.

Fig. 1 shows the process of cycle-slip detection and repair epoch by epoch, which mainly includes two processes, i.e., detection and repair. The detailed process is as follows:

(1) Combine two EWL code-phase combinations and one additional GF phase combination based on time-difference (Equations (3) and (5)).
(2) Estimate the residual ionospheric variation by Equation (7) and correct the GF phase combination by Equation (6).
(3) Update the covariance matrix of the three combinational observations after correcting the residual ionospheric variation (Equation (14)).
(4) Detect cycle slip: if the condition of Equation (13) is satisfied, go to (5); otherwise, terminate the processing and process the next epoch.
(5) Obtain the floating cycle-slip values of three frequencies (Equation (9)) and the corresponding covariance matrix (Equation (10)).
(6) Estimate the best and second-best cycle-slip candidates based on LAMBDA.
(7) Repair cycle slip: if the ratio test is passed (Equation (18)), repair original observations using the best cycle-slip candidates; otherwise, mark this epoch for initialization of the ambiguity solution.

B. DETERMINATION OF THE THRESHOLD VALUE

Unfortunately, the test statistic of Equation (18) does not have an F-distribution [35], [40]–[43] because the two quadratic forms of the test statistic are not independent. This implies that once a value for c is chosen, the F-distribution cannot be used to calculate the corresponding level of significance.

Verhagen [41], [44] proposed a model-driven ratio test with a more flexible approach that uses the fixed failure rate. This approach, which simulates the threshold value under different conditions using large amounts of simulation data, obtains better application results. The procedure for determining the threshold value c based on simulation data is as follows:

(1) Introduce a temporary parameter $u = 1/c$ (called the inverse ratio value in this study) to better reflect the threshold distribution. Choose an acceptable failure rate $P_{\text{fai}} = \beta$ (assume $\beta = 0.01\%$ or here, 0.001%).
(2) For a given model, calculate the failure rate $P_{fai,ILS}$ of cycle-slip repair based on ILS.
(3) If $P_{\text{fai,ILS}} \leq P_{\text{fai}}$, set $c = 1.00$; otherwise, continue with step (4).
(4) Generate N samples of normally distributed float cycle slip: $\Delta \boldsymbol{N}_i \sim N\left(0, \boldsymbol{Q}_{\Delta N}\right), i = 1, \cdots, N$.
(5) Obtain the ILS solutions (best and second-best candidates): $\Delta \boldsymbol{N}^i_{\text{bes}}$, $\Delta \boldsymbol{N}^i_{\text{sec}}$ and

$$r_i = \frac{\left(\Delta \boldsymbol{N}^i_{\text{bes}} - \Delta \boldsymbol{N}'\right)^{\boldsymbol{T}} \boldsymbol{Q}^{-1}_{\Delta \boldsymbol{N}'} \left(\Delta \boldsymbol{N}^i_{\text{bes}} - \Delta \boldsymbol{N}'\right)}{\left(\Delta \boldsymbol{N}^i_{\text{sec}} - \Delta \boldsymbol{N}'\right)^{\boldsymbol{T}} \boldsymbol{Q}^{-1}_{\Delta \boldsymbol{N}'} \left(\Delta \boldsymbol{N}^i_{\text{sec}} - \Delta \boldsymbol{N}'\right)}$$

.
(6) The simulation-based failure rate as a function of u is given by $P_{\text{fai}}(u) = \frac{N_{\text{fai}}}{N}$ with $N_{\text{fai}} = \sum_{i=1}^{N} \omega_i$, where $\omega_i = \begin{cases} 1, \text{if } (r_i \leq u) \\ 0, \text{otherwise.} \end{cases}$

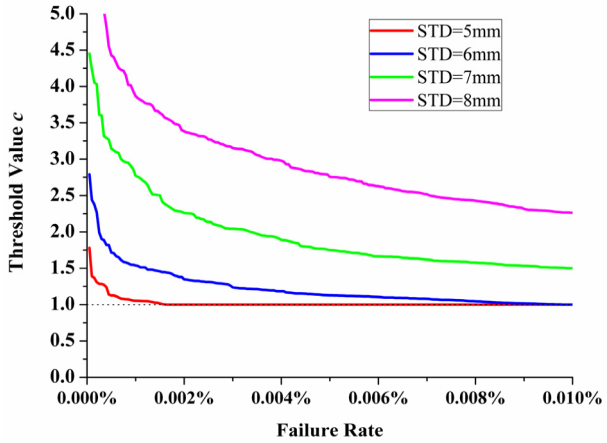

FIGURE 2. Threshold value *c* under different fixed failure rates and different accuracy of ionosphere (STD denotes the accuracy of the residual ionosphere of GF phase combination observations).

TABLE 1. Selection of threshold value *c* under different conditions.

STD[a]	The threshold value *c*					
	99.950% SR[b]	99.975% SR	99.990% SR	99.993% SR	99.996% SR	99.999% SR
≤4 mm	1.00	1.00	1.00	1.00	1.00	1.00
5 mm	1.00	1.00	1.00	1.00	1.00	1.05
6 mm	1.00	1.00	1.00	1.08	1.18	1.54
7 mm	1.01	1.19	1.50	1.62	1.89	2.77
8 mm	1.45	1.75	2.26	2.52	2.98	3.87

[a] STD denotes the accuracy of the residual ionosphere of GF phase combination observations; [b] SR denotes the success rate.

(7) Choose $u_{\min} = \min(r_i) - 10^{-16}$ as this results in $P_{\text{fai}}(u_{\min}) = 0$; $u_{\min} = \max(r_i)$ results in $P_{\text{fai}}(u_{\max}) = P_{\text{fai,ILS}}$.
(8) Use a root-finding method to find a certain existence $u \in [u_{\min}, u_{\max}]$ such that $P_{\text{fai}}(u) = P_{\text{fai}}$.
(9) Determine the threshold value $c = 1/u$.

To obtain the threshold value *c* under different fixed failure rates, a set of simulation data with 2 000 000 samples for every test (total 10 million) is employed. **Fig. 2** shows the threshold value *c* under different fixed failure rates. The STD in **Fig. 2** denotes the accuracy of the residual ionosphere of the GF phase combination observations. The corresponding selection of threshold value *c* is shown in **TABLE 1**. Because the STD of the residual ionospheric variation derived with the commonly used prediction method is generally in the range of 3–7 mm, we just show a selection of values below the threshold of 8 mm.

From **Fig. 2** and **TABLE 1**, the following conclusions can be obtained. (1) The accuracy of the predicted residual ionosphere for correcting the GF phase combination observations is improved, which can greatly enhance the success rate of cycle-slip repair [16]. (2) When the STD of the residual ionosphere of the GF phase combination observations is ≤4 mm, the success rate of cycle-slip repair is >99.999% through selection of the optimal cycle-slip candidates. It means that the optimal cycle-slip candidates using the ILS method are reliable. (3) When the STD of the residual ionosphere of the GF phase combination observations is 5, 6, 7, and 8 mm, to ensure the success rate of cycle-slip repair is maintained at ≥99.99%, the selected threshold value (which is the ratio between the second-best and best integer candidates) should be larger than 1.00, 1.00, 1.50, and 2.26, respectively. Furthermore, to ensure the success rate of cycle-slip repair is maintained at ≥99.999%, the selected threshold value should be larger than 1.05, 1.54, 2.77, and 3.87 when the corresponding STD of the residual ionosphere is 5, 6, 7, and 8 mm, respectively. It should be noted that not all the cycle-slip candidates that satisfy the threshold value are correct, but they can be guaranteed statistically correct.

TABLE 2. STD of the difference between estimated and predicted ionosphere (unit: m).

PRN[a]	STD /m	
	elevation >30°	10°≤elevation≤30°
C01	0.0026	—
C02	0.0037	—
C03	0.0030	—
C04	0.0034	—
C05	—	0.0058
C06	0.0030	0.0059
C07	0.0030	0.0053
C08	0.0036	0.0059
C09	0.0029	0.0053
C10	0.0035	0.0061
C11	0.0033	0.0054
C13	0.0028	0.0052
C14	0.0039	0.0060
Average	0.0032	0.0057

[a] PRN is the satellite number.

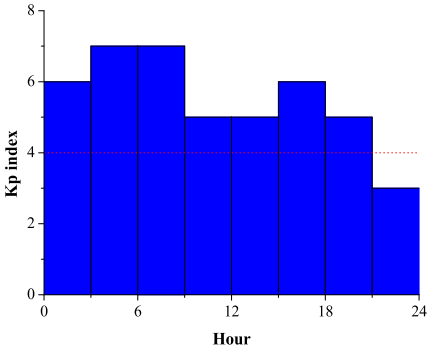

FIGURE 3. Geomagnetic Kp index on August 26, 2018.

IV. EXPERIMENTAL ANALYSIS

To verify the efficiency of the proposed model in repairing cycle slip, a set of real data under conditions of high ionospheric activity on August 26, 2018, were used for

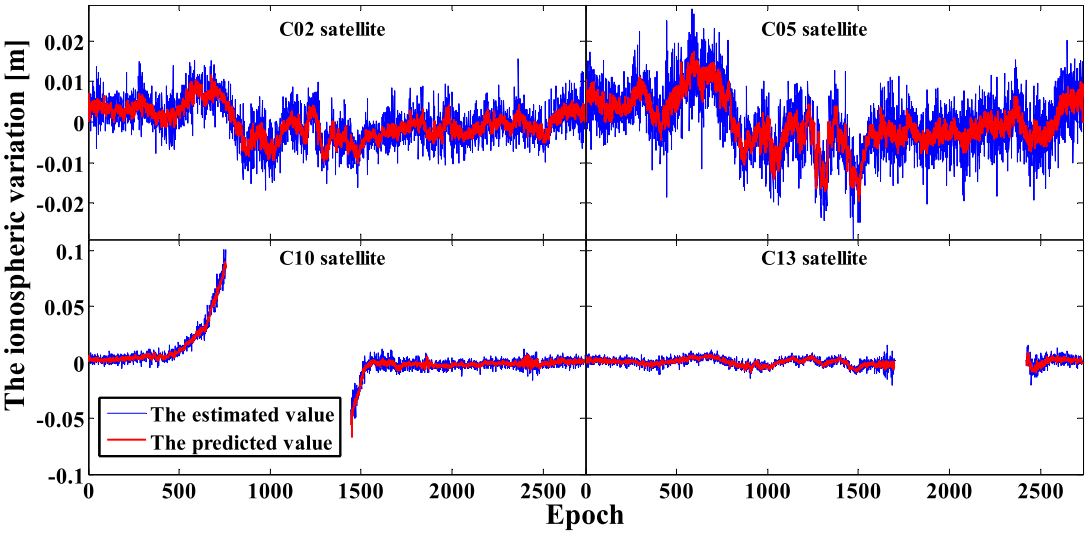

FIGURE 4. Estimated and predicted ionospheric variations (red denotes the predicted value; blue denotes the estimated value): (top left) C02, (top right) C05, (bottom left) C10, and (bottom right) C13.

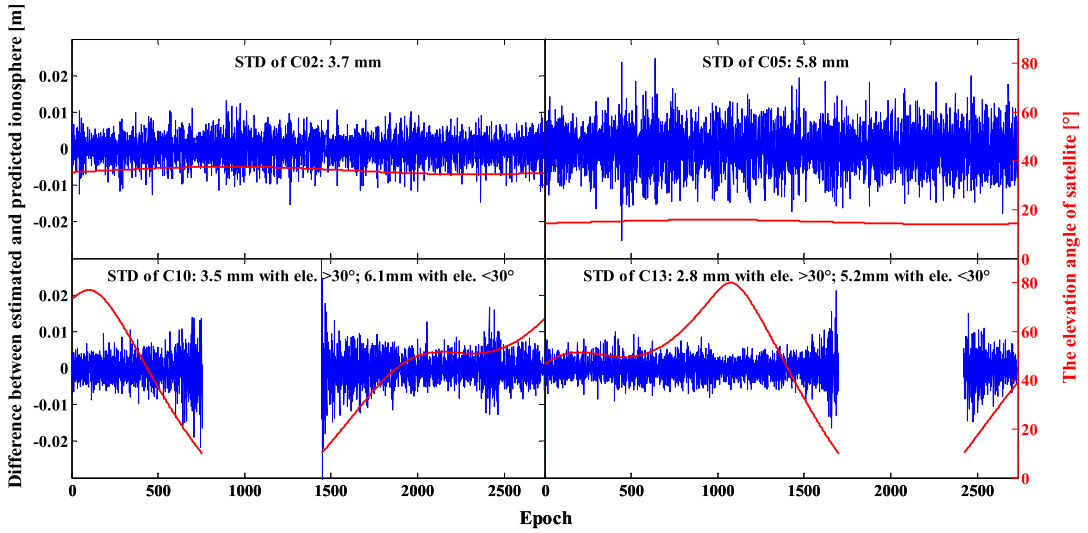

FIGURE 5. Difference between the estimated and predicted ionospheric variations (red denotes the satellite elevation; blue denotes the difference between the estimated and predicted values). (top left) STD of C02 is 3.7mm. (top right) STD of C05 is 5.8mm. (bottom left) STD of C10 is 3.5mm when elevation >30°; which of that is 6.1mm when elevation <30°. (bottom right) STD of C13 is 2.8mm when elevation >30°; which of that is 5.2mm when elevation <30°.

analysis. The ionosphere on this day was active and the corresponding Kp index reached a value of 7 (see **Fig. 3**). The triple-frequency real data were collected at Shanghai (31.10°N, 121.20°E) from the International GNSS Monitoring and Assessment System (iGMAS). The sampling interval was 30 s and the period of observation was 23 h (data for the final hour were missing). Assume that the observation noise of each frequency is $\sigma_\varphi = 0.01$ cycles and $\sigma_p = 0.5$ m in this study [9], [17], [45].

The estimated and predicted ionospheric variations for geosynchronous earth orbit (GEO), inclined geosynchronous satellite orbit (IGSO), and medium earth orbit (MEO) satellites (only the representative C02, C05, C10, and C13 satellites are given) are shown in **Fig. 4**. The corresponding differences between the estimated and predicted values are shown in **Fig. 5**. It can be seen that the simple SWM method produces a reasonable smoothing effect and that it is effective in overcoming the noise of the estimated ionospheric variation, even for the faster change of ionospheric variation associated with IGSO and MEO satellites. Moreover, it is evident from **Fig. 5** that as satellite elevation changes, the differences fluctuate considerably, especially when the satellite elevation is <30°. Fortunately, the differences have no visible systematic deviation. The STD of the corresponding differences for each satellite is shown in the **TABLE 2**. It can be determined that for satellite elevation >30°, the STD of

the predicted ionosphere is in the range 2.6–3.9 mm; for satellite elevation <30°, the STD of the predicted ionospheric variation is in the range 5.2–6.1 mm.

As small values of ratio c are not easy to display, inverse ratio values u ($u_i = 1/c_i$) are used in the analysis because they are sensitive to the details. The corresponding inverse ratio values u for all epoch observations of GEO, IGSO, and MEO satellites are shown in **Fig. 6(a)–(c)**, respectively. As the STD of the predicted ionosphere can reach 6 mm for observations of satellite elevation of <30°, a threshold value of 1.54 was adopted to obtain a cycle-slip-repair success rate of 99.999%.

It is evident from **Fig. 6** that the number of epochs with an inverse ratio value $u > 0.65$ is very small. The corresponding threshold value c is < 1.54, which means the cycle-slip repair solution might be unreliable. It is noted that a small ratio value c does not necessarily mean that the cycle-slip repair is incorrect, just unreliable. More importantly, the cycle-slip repair value used to correct the original observations should satisfy the following conditions: the first one is to satisfy Equation (13), indicating that there might be cycle slip; in addition, Equation (18) needs to be satisfied, indicating that the cycle-slip repair value is reliable. Otherwise, if only one condition of Equations (13) and (18) is satisfied, the cycle slip cannot be repaired because it is unreliable. If the fixed cycle-slip value is repaired compulsively in this epoch, it will contaminate the original carrier-phase observation data.

Fig. 7 shows the inverse ratio value of all epochs and the corresponding satellite elevation. It is evident that the inverse ratio values are larger for smaller satellite elevation. It means that the cycle-slip repair solution is not very reliable for small satellite elevations. The reason is mainly attributable to the large ionospheric variation when the satellite elevation is small. In addition, the inverse ratio values of satellite C05 show a large increase in comparison with other satellites. The main reason is that the elevation angle of satellite C05 is only in the range 14°–16°.

Fig. 8 shows the floating errors of the estimations of EWL_1, EWL_2, and ΔN_3 for the C02, C05, C10, and C13 satellites. It is evident that the floating errors of most epochs for all satellites are no larger than 0.5 cycles, except for the 445^{th} and 446^{th} epochs of the C05 satellite, demonstrating efficient and accurate detection of cycle slip. Although satellite C05 was found to have a possible cycle slip in two epochs, the proposed method does not repair the original observation. This is mainly because the corresponding ratio values are all < 1.54, indicating that the cycle-slip repair value is unreliable. Compared with direct rounding, the efficiency of repairing cycle slip using the ILS method is superior.

No cycle slip existed in the original phase observations. To evaluate the performance of the proposed method, we simulated four types of cycle slip on the original carrier-phase observations, including small (S in **TABLE 3**), large (L in **TABLE 3**), approximate (A in **TABLE 3**), and particular (P in **TABLE 3**, a cycle-slip group insensitive to partial cycle-slip detection amount) cycle slips. **TABLE 3** shows the

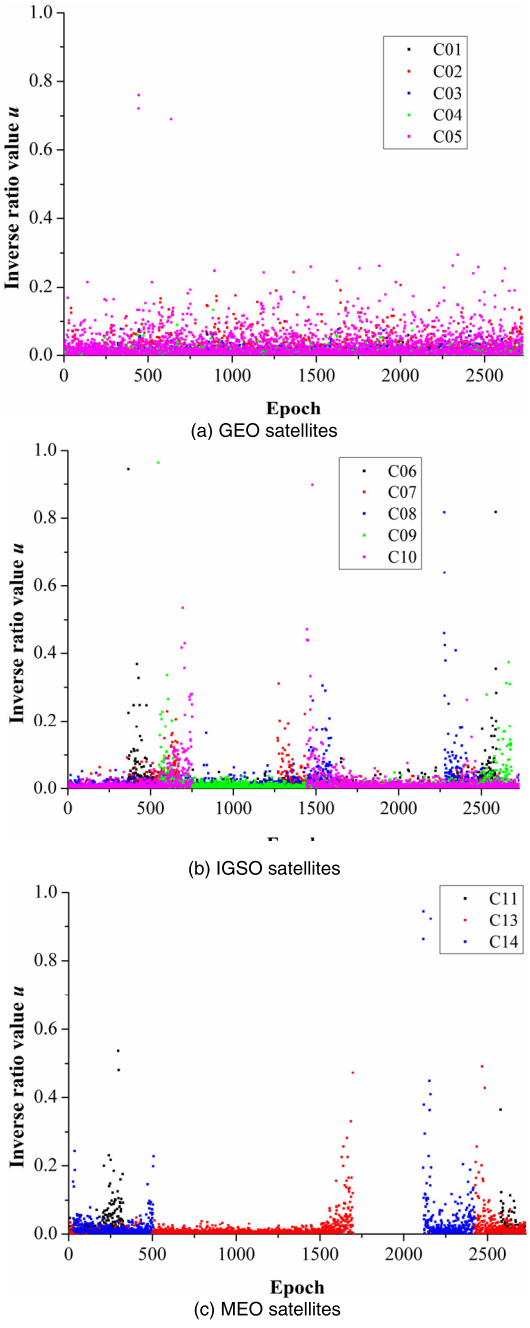

FIGURE 6. Inverse ratio values u ($u = 1/c$. c is the ratio between the second-best and best cycle-slip candidates): (a) GEO satellites, (b) IGSO satellites, and (c) MEO satellites.

location, added size of cycle slip, cycle-slip type, floating and fixed estimations of cycle slip, and corresponding ratio value c. It is evident that the fixed estimations of cycle slip of all epochs for all satellites using the ILS method is repaired correctly, even the 445^{th} and 446^{th} epochs of satellite C05 and the 2163^{rd} epoch of satellite C14. However, the corresponding ratio value of those three epochs is smaller than the threshold value of 1.54. On the one hand, to guarantee a cycle-slip-repair success rate of 99.999%, we recommend only marking these cycle slips without repair in this situation,

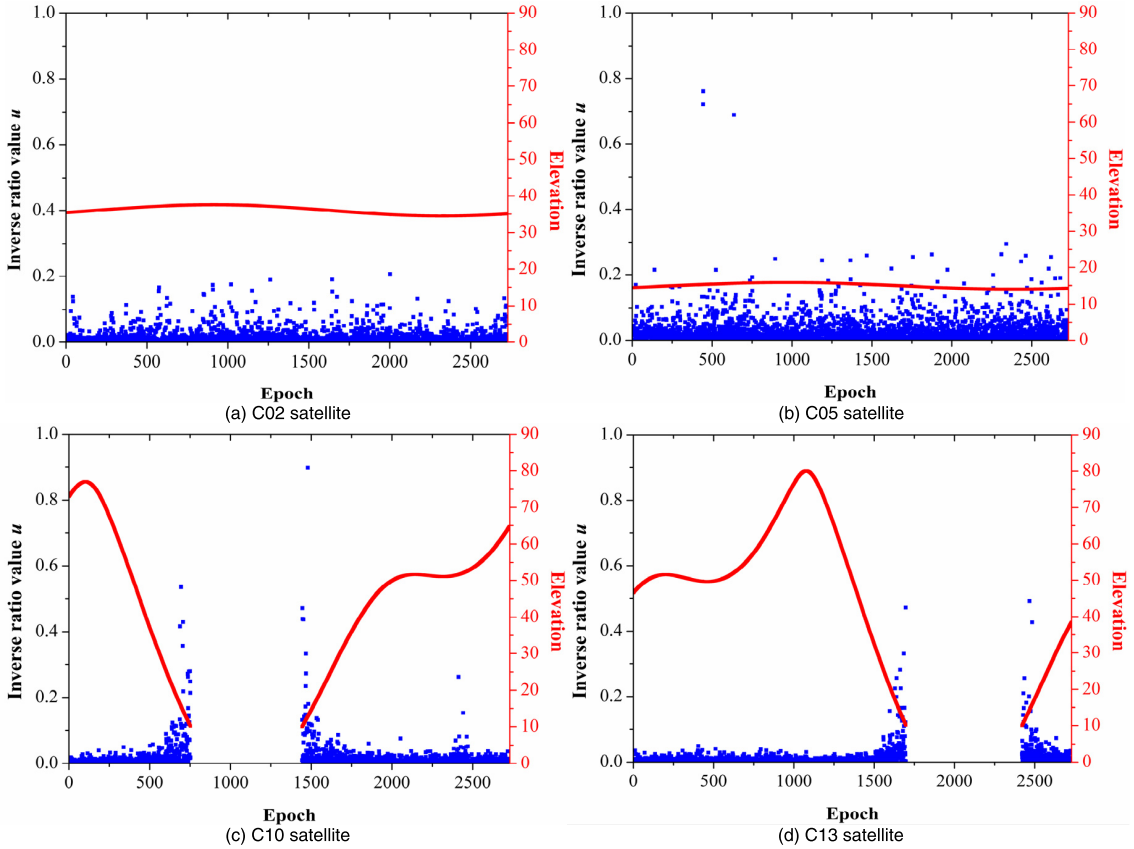

FIGURE 7. Inverse ratio value u and satellite elevation: (a) C02, (b) C05, (c) C10 and (d) C13. It is evident that the inverse ratio value u has large fluctuation when the satellite elevation is <30°, especially the C05 satellite.

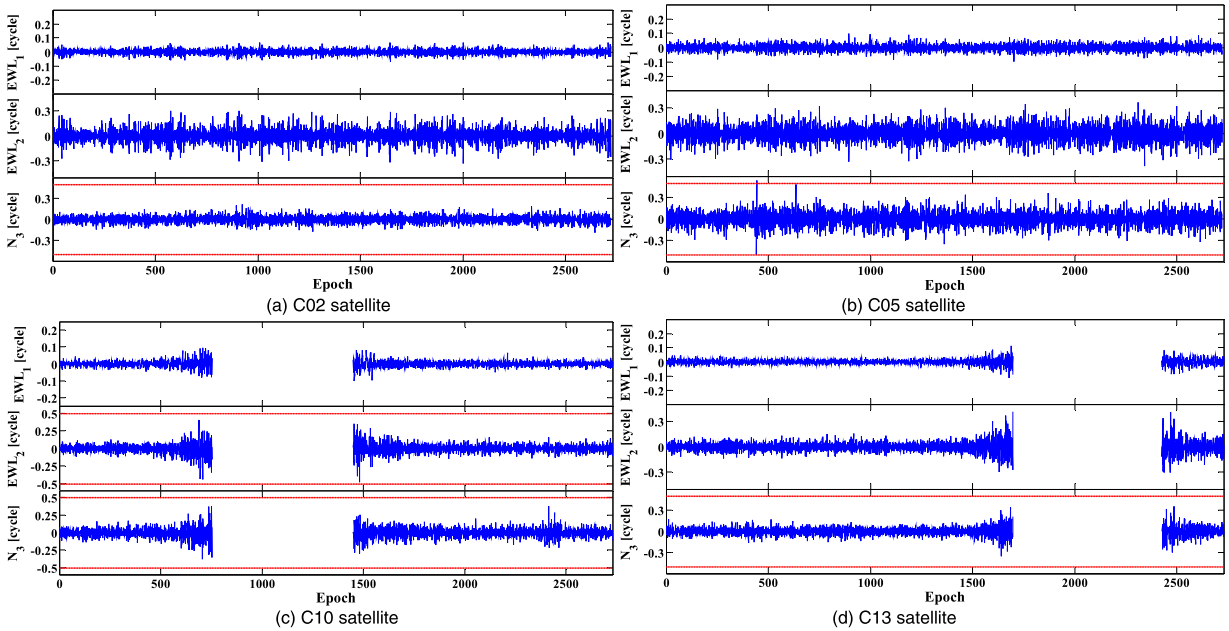

FIGURE 8. Cycle-slip detection value: (a) C02, (b) C05, (c) C10 and (d) C13. The EWL_1 and EWL_2 are the EWL code-phase combinations (0, −1, 1) and (1, 4, −5), respectively (unit: cycles). N_3 is the floating cycle-slip estimations of the third frequency (unit: cycles).

even if the fixed cycle-slip estimations might be correct. If the fixed cycle-slip estimations were repaired compulsively in this epoch, it could contaminate the original carrier-phase observation data. Therefore, only the epoch positions that might have a cycle slip are marked for ambiguity initialization in precise positioning. On the other hand, to guarantee a

TABLE 3. Simulated results of cycle-slip detection and repair using real data (23h; sampling interval is 30 s).

PRN [a]	Epoch	Cycle slip value	Cycle slip type [b]	Floating estimation value of cycle-slip			Fixed estimation value of cycle-slip			Ratio value
				ΔN_1 /cycle	ΔN_2 /cycle	ΔN_3 /cycle	ΔN_1 /cycle	ΔN_2 /cycle	ΔN_3 /cycle	
C02	300	(1,0,0)	P&S	0.977	-0.023	-0.027	1	0	0	632.22
C02	600	(0,1,1)	P&S	-0.042	0.994	0.995	0	1	1	41.48
C02	900	(1,1,1)	P&S	0.857	0.860	0.875	1	1	1	44.50
C02	1200	(763,590,0)	P&L	762.793	589.826	-0.161	763	590	0	85.77
C02	1500	(100,100,100)	P&L	99.929	99.947	99.949	100	100	100	763.36
C02	1800	(99,101,100)	L&A	98.950	100.966	99.938	99	101	100	43.85
C05	445	(1,0,0)	P&S	1.184	-0.029	-0.078	1	0	0	**1.39**
C05	446	(0,1,1)	P&S	0.244	1.311	1.254	0	1	1	**1.32**
C05	1000	(1,1,1)	P&S	0.004	0.240	0.208	1	1	1	78.35
C05	1300	(763,590,0)	P&L	762.931	589.942	-0.067	763	590	0	376.25
C05	1600	(100,100,100)	P&L	100.072	100.063	100.066	100	100	100	662.40
C05	1900	(99,101,100)	L&A	99.040	101.044	100.034	99	101	100	226.10
C10	500	(1,0,0)	P&S	1.040	0.034	0.021	1	0	0	170.13
C10	700	(0,1,1)	P&S	0.494	1.370	1.387	0	1	1	160.97
C10	1500	(1,1,1)	P&S	1.412	1.307	1.314	1	1	1	100.37
C10	1800	(763,590,0)	P&L	763.205	590.136	0.145	763	590	0	68.85
C10	2100	(100,100,100)	P&L	100.023	100.030	100.018	100	100	100	208.90
C10	2400	(99,101,100)	L&A	98.904	100.917	99.915	99	101	100	505.38
C13	600	(1,0,0)	P&S	0.929	-0.049	-0.050	1	0	0	657.95
C13	900	(0,1,1)	P&S	-0.136	0.903	0.878	0	1	1	96.68
C13	1200	(1,1,1)	P&S	1.166	1.135	1.132	1	1	1	457.25
C13	1500	(763,590,0)	P&L	763.222	590.178	0.172	763	590	0	154.92
C13	2500	(100,100,100)	P&L	100.047	100.035	100.019	100	100	100	82.09
C13	2700	(99,101,100)	L&A	99.282	101.236	100.258	99	101	100	49.65
C14	2163	(1,0,0)	P&S	0.443	-0.551	-0.527	1	0	0	**1.08**

[a] PRN is the satellite number. [b] P denotes particular cycle slip, S denotes small cycle slip, L denotes large cycle slip and A denotes approximate cycle slip.

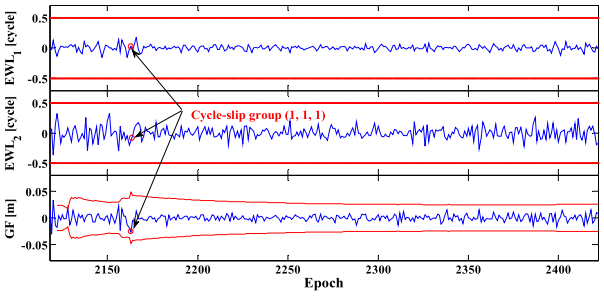

FIGURE 9. Real cycle-slip detection results with cycle-slip group (1, 1, 1) in the 2163rd epoch of the C14 satellite. The EWL_1 and EWL_2 are the EWL code-phase combinations (0, −1, 1) and (1, 4, −5), respectively (unit: cycles). GF denotes the GF combination (1, −1, 0) (unit: m).

cycle-slip-repair success rate of 99.99% (the threshold value of 1.00), the best cycle-slip candidates are considered to be reliable.

For more comprehensive verification of the performance of the proposed method, two special cycle-slip groups (1, 1, 1) and (1, 0, 0) were added to all epochs of each satellite, except the first five epochs that are more difficult to detect and repair and thus have often been used in other studies to verify performance [22], [46], [47]. The experimental results in **TABLE 4** show that the cycle-slip groups (1, 1, 1) and (1, 0, 0) of all epochs were detected successfully and repaired correctly, except cycle-slip group (1, 1, 1) in the 2163rd epoch of the C14 satellite. Moreover, the success rate of cycle-slip repair is 99.997% in this test. The corresponding cycle-slip detection results are shown in **Fig. 9**. It is evident from **Fig. 9** that the cycle-slip detection values in the 2163rd epoch of the C14 satellite are less than the threshold values, resulting in the missed detection. The reason for this failure is that the ionospheric variation of the 2163rd epoch was disturbed, causing the GF phase combination to be insensitive to

TABLE 4. Statistical results of cycle-slip repair using triple-frequency observations (23h; sampling interval is 30 s).

PRN	Total number of epochs	Fail detection /Wrong repair Cycle-slip group (1, 1, 1)	Fail detection /Wrong repair Cycle-slip group (1, 0, 0)
C01	2729	0 / 0	0 / 0
C02	2729	0 / 0	0 / 0
C03	2729	0 / 0	0 / 0
C04	2729	0 / 0	0 / 0
C05	2726	0 / 0	0 / 0
C06	2222	0 / 0	0 / 0
C07	2134	0 / 0	0 / 0
C08	2048	0 / 0	0 / 0
C09	2133	0 / 0	0 / 0
C10	2039	0 / 0	0 / 0
C11	479	0 / 0	0 / 0
C13	2007	0 / 0	0 / 0
C14	798	1 / 1	0 / 0
Sum	27502	1 / 1	0 / 0

cycle-slip group (1, 1, 1), leading to failure of repair. The same result was also obtained in a previous study [46].

V. CONCLUSIONS AND PROSPECTS

An improved cycle-slip repair model for BDS triple-frequency undifferenced observations was proposed in this contribution. First, a model consisting of three linearly independent combined observations was adopted: two EWL code-phase combinations and one additional GF phase combination. Considering the nonnegligible influence of the residual ionospheric variation on the accuracy of the GF phase combinations and the floating cycle-slip estimation, the simple highly efficient SWM method was adopted to correct the ionospheric variation at the current epoch using the predicted ionospheric variations, which can ensure the corrected GF combination observations followed a normal distribution. Then, it was necessary to update the constructed covariance matrix of the floating cycle-slip estimations in real time depending on the accuracy of the residual ionosphere over a certain period, such that the optimal solution of the fixed cycle slip could be solved using the ILS-based LAMBDA method. Finally, a set of real observations under active ionospheric conditions was used for analysis of the model performance. The results showed the success rate of cycle-slip repair using the improved model was 99.997%, even under the conditions of an active ionosphere and a low satellite elevation. Unfortunately, one cycle-slip group (1, 1, 1) of the C14 satellite was not detected successfully and repaired correctly because of insensitivity to the GF phase combination under bad observation conditions.

A criterion for correctly repairing cycle slip was also proposed, and a selection of threshold values for different residual ionosphere accuracies and different success rates of repairing cycle slip were given in **TABLE 1**. Analysis of large amounts of simulated data revealed the following. (1) When the STD of the residual ionospheric variations of GF phase observations is $\leq$4 mm, the success rate of cycle-slip repair is $>$99.999% through selection of the optimal cycle-slip candidate using the ILS method. (2) When the STD of the residual ionospheric variations of GF phase observations is 5, 6, 7, and 8 mm, the selected threshold value should be 1.00, 1.00, 1.50, and 2.26, respectively, to ensure a success rate of cycle-slip repair of $>$99.99%. (3) Furthermore, to ensure a success rate of cycle-slip repair of $>$99.999%, the selected threshold value should be 1.05, 1.54, 2.77, and 3.87 when the corresponding STD of the residual ionosphere is 5, 6, 7, and 8 mm, respectively.

In this analysis, we did not consider the correlation between epochs and parameters, nor did we consider the non-integer case of cycle slip; both subjects should be investigated in future study.

ACKNOWLEDGMENT

The author is grateful to the iGMAS community for providing the BDS data used in this study. The authors are grateful to reviewers for providing many insightful and constructive suggestions.

REFERENCES

[1] Y. Feng and B. Li, "A benefit of multiple carrier GNSS signals: Regional scale network-based RTK with doubled inter-station distances," *J. Spatial Sci.*, vol. 53, no. 2, pp. 135–147, 2008.
[2] X. Zhang and P. Li, "Benefits of the third frequency signal on cycle slip correction," *GPS Solutions*, vol. 20, pp. 451–460, Jul. 2015.
[3] J. Li, J. Yang, J. Xu, H. He, and H. Guo, "Real-time cycle-slip detection and repair based on code-phase combinations for GNSS triple-frequency undifferenced observations," *Acta Geodaetica et Cartographica Sinica*, vol. 40, no. 6, pp. 717–722, 2011.
[4] J. Li, Y. Yang, H. He, and H. Guo, "An analytical study on the carrier-phase linear combinations for triple-frequency GNSS," *J. Geodesy*, vol. 91, pp. 151–166, Feb. 2017.
[5] M. Cocard, S. Bourgon, O. Kamali, and P. Collins, "A systematic investigation of optimal carrier-phase combinations for modernized triple-frequency GPS," *J. Geodesy*, vol. 82, no. 9, pp. 555–564, 2008.
[6] T. Richert and N. El-Sheimy, "Optimal linear combinations of triple frequency carrier phase data from future global navigation satellite systems," *GPS Solutions*, vol. 11, pp. 11–19, Jan. 2007.
[7] L. Urquhart, "An analysis of multi-frequency carrier phase linear combinations for GNSS," Univ. New Brunswick, Fredericton, NB, Canada, Tech. Rep. 263, 2009.
[8] G. Blewitt, "An automatic editing algorithm for GPS data," *Geophys. Res. Lett.*, vol. 17, pp. 199–202, Mar. 1990.
[9] Z. Liu, "A new automated cycle slip detection and repair method for a single dual-frequency GPS receiver," *J. Geodesy*, vol. 85, pp. 171–183, Mar. 2010.
[10] W. Melbourne, "The case for ranging in GPS-based geodetic systems," in *Proc. 1st Int. Symp. Precise Positioning Global Positioning Syst.*, 1985, pp. 373–386.
[11] G. Wübbena, "Software developments for geodetic positioning with GPS using TI 4100 code and carrier measurements," in *Proc. 1st Int. Symp. Precise Positioning Global Positioning Syst.*, 1985, pp. 403–412.
[12] L. Huang, Z. Lu, G. Zhai, Y. Ouyang, M. Huang, X. Lu, T. Wu, and K. Li, "A new triple-frequency cycle slip detecting algorithm validated with BDS data," *GPS Solutions*, vol. 20, pp. 761–769, Oct. 2015.
[13] C. Cai, Z. Liu, P. Xia, and W. Dai, "Cycle slip detection and repair for undifferenced GPS observations under high ionospheric activity," *GPS Solutions*, vol. 17, no. 2, pp. 247–260, Jul. 2013.
[14] G. Chang, T. Xu, Y. Yao, and Q. Wang, "Adaptive Kalman filter based on variance component estimation for the prediction of ionospheric delay in aiding the cycle slip repair of GNSS triple-frequency signals," *J. Geodesy*, vol. 92, no. 11, pp. 1241–1253, 2018.

[15] M. C. de Lacy, M. Reguzzoni, and F. Sansò, "Real-time cycle slip detection in triple-frequency GNSS," *GPS Solutions*, vol. 16, pp. 353–362, Jul. 2012.
[16] Y. Yifei, C. Xinyun, C. Guobin, and G. Hongsuo, "Accuracy analysis of ionospheric prediction models for repairing cycle slips for beidou triple-frequency observations," *J. Navigat.*, pp. 1–20, May 2019. doi: 10.1017/S0373463319000456.
[17] Y.-F. Yao, J.-X. Gao, J. Wang, H. Hu, and Z.-K. Li, "Real-time cycle-slip detection and repair for BeiDou triple-frequency undifferenced observations," *Surv. Rev.*, vol. 48, no. 350, pp. 367–375, 2016.
[18] Q. Zhao, B. Sun, Z. Dai, Z. Hu, C. Shi, and J. Liu, "Real-time detection and repair of cycle slips in triple-frequency GNSS measurements," *GPS Solutions*, vol. 19, no. 3, pp. 381–391, Jul. 2015.
[19] D. Kim, J. Song, S. Yu, C. Kee, and M. Heo, "A new algorithm for high-integrity detection and compensation of dual-frequency cycle slip under severe ionospheric storm conditions," *Sensors*, vol. 18, no. 11, p. 3654, 2018.
[20] W. Liu, X. Jin, M. Wu, J. Hu, and Y. Wu, "A new real-time cycle slip detection and repair method under high ionospheric activity for a triple-frequency GPS/BDS receiver," *Sensors*, vol. 18, no. 2, p. 427, 2018.
[21] D. Zhao, C. M. Hancock, G. W. Roberts, and S. Jin, "Cycle slip detection during high ionospheric activities based on combined triple-frequency GNSS signals," *Remote Sens.*, vol. 11, no. 3, p. 250, 2019.
[22] X. Gu and B. Zhu, "Detection and correction of cycle slip in triple-frequency GNSS positioning," *IEEE Access*, vol. 5, pp. 12584–12595, 2017.
[23] B. Li, Y. Qin, Z. Li, and L. Lou, "Undifferenced cycle slip estimation of triple-frequency BeiDou signals with ionosphere prediction," *Marine Geodesy*, vol. 39, no. 5, pp. 348–365, 2016.
[24] B. Li, Y. Qin, and T. Liu, "Geometry-based cycle slip and data gap repair for multi-GNSS and multi-frequency observations," *J. Geodesy*, vol. 93, no. 3, pp. 399–417, Mar. 2019.
[25] B. Li, S. Verhagen, and P. J. G. Teunissen, "Robustness of GNSS integer ambiguity resolution in the presence of atmospheric biases," *GPS Solutions*, vol. 18, pp. 283–296, Apr. 2014.
[26] J.-P. Montillet, L. K. Bonenberg, C. M. Hancock, and G. W. Roberts, "On the improvements of the single point positioning accuracy with Locata technology," *GPS solutions*, vol. 18, pp. 273–282, Apr. 2014.
[27] J.-P. Montillet, G. W. Roberts, C. Hancock, X. Meng, O. Ogundipe, and J. Barnes, "Deploying a Locata network to enable precise positioning in urban canyons," *J. Geodesy*, vol. 83, pp. 91–103, Feb. 2009.
[28] L. Tang, K. Zheng, and X. Li, "Analysis of geometry-free residuals in case of traveling ionosphere disturbances and their impact cycle slip detection," *GPS Solutions*, vol. 21, pp. 1221–1226, Jul. 2017.
[29] C. Deng, J. Cui, W. Tang, X. Zou, and L. Shu, "Reliable real-time triple-frequency cycle slip detection and recovery with adaptive detection thresholds," *Meas. Sci. Technol.*, vol. 30, no. 5, 2019, Art. no. 055007.
[30] F. Zangeneh-Nejad, A. R. Amiri-Simkooei, M. A. Sharifi, and J. Asgari, "Cycle slip detection and repair of undifferenced single-frequency GPS carrier phase observations," *GPS Solutions*, vol. 21, no. 4, pp. 1593–1603, Oct. 2017.
[31] B. Li, T. Liu, L. Nie, and Y. Qin, "Single-frequency GNSS cycle slip estimation with positional polynomial constraint," *J. Geodesy*, pp. 1–23, Jul. 2019. doi: 10.1007/s00190-019-01281-7.
[32] B. Li, Y. Feng, W. Gao, and Z. Li, "Real-time kinematic positioning over long baselines using triple-frequency BeiDou signals," *IEEE Trans. Aerosp. Electron. Syst.*, vol. 51, no. 4, pp. 3254–3269, Oct. 2015.
[33] P. J. G. Teunissen, "The least-squares ambiguity decorrelation adjustment: A method for fast GPS integer ambiguity estimation," *J. Geodesy*, vol. 70, no. 1, pp. 65–82, 1995.
[34] P. J. G. Teunissen, "The parameter distributions of the integer GPS model," *J. Geodesy*, vol. 76, pp. 41–48, Jan. 2002.
[35] S. Verhagen, "Integer ambiguity validation: An open problem?" *GPS Solutions*, vol. 8, pp. 36–43, Apr. 2004.
[36] S. Han and C. Rizos, "Validation and rejection criteria for integer least-squares estimation," *Surv. Rev.*, vol. 33, no. 260, pp. 375–382, 1996.
[37] A. Parkins, "Increasing GNSS RTK availability with a new single-epoch batch partial ambiguity resolution algorithm," *GPS Solutions*, vol. 15, no. 4, pp. 391–402, Oct. 2011.
[38] M. Wei, "Fast ambiguity resolution using an integer nonlinear programming method," in *Proc. ION GPS*, 1995, pp. 1101–1110.
[39] J. Wang, M. P. Stewart, and M. Tsakiri, "A discrimination test procedure for ambiguity resolution on-the-fly," *J. Geodesy*, vol. 72, no. 11, pp. 644–653, Nov. 1998.
[40] P. J. Teunissen, "GPS carrier phase ambiguity fixing concepts," in *GPS for Geodesy*. Berlin, Germany: Springer, 1998, pp. 319–388.
[41] A. A. Verhagen, "The GNSS integer ambiguities: Estimation and validation," Ph.D. dissertation, Delft Univ. Technol., Delft, The Netherland, 2005.
[42] S. Verhagen and P. Teunissen, "On the foundation of the popular ratio test for GNSS ambiguity resolution," in *Proc. 17th Int. Tech. Meeting Satell. Division Inst. Navigat. (ION GNSS)*, 2004, pp. 2529–2540.
[43] P. J. G. Teunissen and P. F. De Bakker, "Single-receiver single-channel multi-frequency GNSS integrity: Outliers, slips, and ionospheric disturbances," *J. Geodesy*, vol. 87, no. 2, pp. 161–177, Feb. 2013.
[44] S. Verhagen and P. J. G. Teunissen, "The ratio test for future GNSS ambiguity resolution," *GPS Solutions*, vol. 17, no. 4, pp. 535–548, 2013.
[45] K. Wang and M. Rothacher, "Ambiguity resolution for triple-frequency geometry-free and ionosphere-free combination tested with real data," *J. Geodesy*, vol. 87, pp. 539–553, Jun. 2013.
[46] T. Zeng, L. Sui, Y. Xu, X. Jia, G. Xiao, Y. Tian, and Q. Zhang, "Real-time triple-frequency cycle slip detection and repair method under ionospheric disturbance validated with BDS data," *GPS Solutions*, vol. 22, p. 62, Jul. 2018.
[47] T. Li and S. Melachroinos, "An enhanced cycle slip repair algorithm for real-time multi-GNSS, multi-frequency data processing," *GPS Solutions*, vol. 23, p. 1, Jan. 2019.

YIFEI YAO received the Ph.D. degree in geodesy and survey engineering field from the China University of Mining and Technology, Xuzhou, China, in 2017. He is currently a Lecturer with the College of Water Resources and Architectural Engineering, Northwest A&F University. His current research interests include cycle-slip detection and repair, analysis and processing of BeiDou triple-frequency data, and GNSS high-precision positioning.

XIN ZHANG received the Ph.D. degree in hydrology and water resources from Northwest A&F University, Yangling, China, in 2005, where he is currently a Professor with the College of Water Resources and Architectural Engineering. His current research interests include hydrology and water resources, and 3S technology and application.

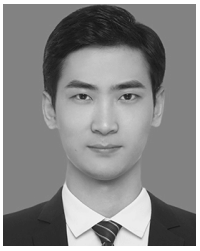

XINYUN CAO received the Ph.D. degree in geodesy and survey engineering field from Wuhan University, Wuhan, China, in 2018. He is currently a Lecturer with the School of Geography Science, Nanjing Normal University. His current research interest includes multi-GNSS high-precision positioning and its applications.